

Published in final edited form as:

*Med Image Anal.* 2013 April ; 17(3): 325–336. doi:10.1016/j.media.2012.12.001.

## Reliable estimation of Incoherent Motion parametric maps from diffusion-weighted MRI using fusion bootstrap moves

Moti Freiman<sup>a</sup>, Jeannette M. Perez-Rossello<sup>b</sup>, Michael J. Callahan<sup>b</sup>, Stephan D. Voss<sup>b</sup>, Kirsten Ecklund<sup>b</sup>, Robert V. Mulkern<sup>b</sup>, and Simon K. Warfield<sup>a</sup>

Moti Freiman: moti.freiman@childrens.harvard.edu; Jeannette M. Perez-Rossello: jeannette.perez-rossello@childrens.harvard.edu; Michael J. Callahan: michael.callahan@childrens.harvard.edu; Stephan D. Voss: stephan.voss@childrens.harvard.edu; Kirsten Ecklund: kirsten.ecklund@childrens.harvard.edu; Robert V. Mulkern: robert.mulkern@childrens.harvard.edu; Simon K. Warfield: simon.warfield@childrens.harvard.edu

<sup>a</sup>Computational Radiology Laboratory, Boston Children's Hospital, Harvard Medical School, 300 Longwood Avenue, Boston, MA 02115, USA

<sup>b</sup>Department of Radiology, Children's Hospital Boston, Harvard Medical School, 300 Longwood Avenue, Boston, MA 02115, USA

### Abstract

Diffusion-weighted MRI has the potential to provide important new insights into physiological and microstructural properties of the body. The Intra-Voxel Incoherent Motion (IVIM) model relates the observed DW-MRI signal decay to parameters that reflect blood flow in the capillaries ( $D^*$ ), capillaries volume fraction ( $f$ ), and diffusivity ( $D$ ). However, the commonly used, independent voxel-wise fitting of the IVIM model leads to imprecise parameter estimates, which has hampered their practical usage.

In this work, we improve the precision of estimates by introducing a spatially-constrained Incoherent Motion (IM) model of DW-MRI signal decay. We also introduce an efficient iterative “fusion bootstrap moves” (FBM) solver that enables precise parameter estimates with this new IM model. This solver updates parameter estimates by applying a binary graph-cut solver to fuse the current estimate of parameter values with a new proposal of the parameter values into a new estimate of parameter values that better fits the observed DW-MRI data. The proposals of parameter values are sampled from the independent voxel-wise distributions of the parameter values with a model-based bootstrap resampling of the residuals.

We assessed both the improvement in the precision of the Incoherent Motion parameter estimates and the characterization of heterogeneous tumor environments by analyzing simulated and in-vivo abdominal DW-MRI data of 30 patients, and in-vivo DW-MRI data of three patients with musculoskeletal lesions. We found our IM-FBM reduces the relative root mean square error of the  $D^*$  parameter estimates by 80%, and of the  $f$  and  $D$  parameter estimates by 50% compared to the IVIM model with the simulated data. Similarly, we observed that our IM-FBM method significantly reduces the coefficient of variation of parameter estimates of the  $D^*$  parameter by 43%, the  $f$  parameter by 37%, and the  $D$  parameter by 17% compared to the IVIM model (paired Student's t-test,  $p < 0.0001$ ). In addition, we found our IM-FBM method improved the

© 2012 Elsevier B.V. All rights reserved.

Correspondence to: Moti Freiman, moti.freiman@childrens.harvard.edu.

**Publisher's Disclaimer:** This is a PDF file of an unedited manuscript that has been accepted for publication. As a service to our customers we are providing this early version of the manuscript. The manuscript will undergo copyediting, typesetting, and review of the resulting proof before it is published in its final citable form. Please note that during the production process errors may be discovered which could affect the content, and all legal disclaimers that apply to the journal pertain.

characterization of heterogeneous musculoskeletal lesions by means of increased contrast-to-noise ratio of 19.3%.

The IM model and FBM solver combined, provide more precise estimate of the physiological model parameter values that describing the DW-MRI signal decay and a better mechanism for characterizing heterogeneous lesions than does the independent voxel-wise IVIM model.

## Keywords

Diffusion-weighted imaging; Intra-voxel incoherent motion; Spatial homogeneity prior; Bayesian estimation; Graph min-cut

## 1. Introduction

Diffusion-weighted MRI (DW-MRI) of the body is a non-invasive imaging technique sensitive to the incoherent motion of water molecules inside the area of interest. This motion is known to be a combination of a slow diffusion component associated with the Brownian motion of water molecules, and a fast diffusion component associated with the bulk motion of intravascular molecules in the micro-capillaries. These phenomena are characterized through the so-called, Intra-Voxel Incoherent Motion (IVIM) model with the slow diffusion ( $D$ ); the fast diffusion ( $D^*$ ) as decay rate parameters; and the fractional contribution ( $f$ ) of each motion to the DW-MRI signal decay (Le Bihan, 2008; Le Bihan et al., 1988; Koh et al., 2011).

IVIM model parameters have recently shown promise as quantitative imaging biomarkers for various clinical applications in the body including differential analysis of tumors (Sigmund et al., 2011; Re et al., 2011; Klauss et al., 2011; Chandarana et al., 2011; Gloria et al., 2010; Lemke et al., 2009), the assessment of liver cirrhosis (Luciani et al., 2008; Patel et al., 2010), and Crohn's disease (Freiman et al., 2012a).

A key limitation of the IVIM model is that it is an independent voxel-wise model. It models only signal decay related to intra-voxel incoherent motion of the water molecules, while both inter- and intra-voxel incoherent motion of water molecules are related to the DW-MRI signal decay. Moreover, the utility of IVIM parametric imaging with DW-MRI is diminished by a lack of verified methods for producing reliable estimates of both fast and slow diffusion parameters from the DW-MRI signal (Koh et al., 2011).

Specifically, reliable estimates of IVIM model parameters are difficult to obtain because of 1) the non-linearity of the IVIM model; 2) the limited number of DW-MRI images as compared to the number of the IVIM model parameters, and; 3) the low signal-to-noise ratio (SNR) observed in body DW-MRI.

In current practice, there are four approaches that will increase the reliability of incoherent motion parameter estimates to varying degrees.

1. Approximate the non-linear DW-MRI signal decay by a log-linear model with the apparent diffusion coefficient (ADC) as the decay rate parameter (Stejskal and Tanner, 1965). However, this simplified model precludes the independent characterization of slow diffusion and fast diffusion components - a process essential to accurately quantifying biological phenomena taking place inside the body.
2. Increase the DW-MRI SNR by acquiring multiple DW-MRI images from the patient; next, average these results, and then use the averaged DW-MRI signal to

estimate IVIM model parameters. However, this requires substantially increased acquisition times - an undesirable outcome, especially in children, who generally have difficulty in remaining still for long periods of time (Koh et al., 2011).

3. Increase the DW-MRI SNR by averaging the DW-MRI signal over a region of interest (ROI), effectively yielding more reliable IVIM parameter estimates as used by Zhang et al. in their DW-MRI acquisition optimization study (Zhang et al., 2012). Unfortunately, by averaging the signal over a ROI, the estimated parameters do not reflect critical heterogeneous environments such as the necrotic and viable parts of tumors.
4. Bayesian model fitting, proposed by Neil et al. (Neil and Bretthorst, 1993), and recently used by Koh et al. (Koh et al., 2011) aims to increase the reliability of IVIM parameter estimates by calculating the probability distribution function of each parameter rather than by calculating point estimates, as is done using maximum-likelihood estimators. However, this method considers the information at each voxel independently, effectively ignoring its spatial context. Moreover, it requires numerical integration of the marginal posterior probabilities over the possible ranges of parameter values, which are sensitive both to discretization/sampling effects and to the chosen integration limits (Behrens et al., 2003).

In this work, we present a new model of DW-MRI signal decay that accounts for both inter- and intra-voxel incoherent motion of the water molecules (IM) by introducing a model of spatial homogeneity to the IVIM model of DW-MRI signal decay. Essentially, our IM model produces estimates of Incoherent Motion model parameters for all voxels simultaneously, rather than solving for each voxel independently. As a result, we increase the reliability of the incoherent motion parameter estimates from the DW-MRI data without acquiring additional data or losing spatial sensitivity. Figure 1 depicts the graphical models previously used to estimate the fast and slow diffusion parameters from DW-MRI data (a–c) compared to the model proposed in this work (d).

Bayesian estimation of Markov Random Field (MRF) models with spatial homogeneity as a prior term has been widely used in computer vision applications since its introduction by Geman and Geman (Geman and Geman, 1984). The equivalence between MRFs and Gibbs distributions established by Hamersley and Clifford (Winkler, 2003) also enabled the modeling of variety of computer vision problems such as energy minimization tasks within the Bayesian framework (Geman and Geman, 1984).

The optimization of MRF-related energy functions is challenging, however, due to the large number of variables that must be optimized simultaneously, especially when compared to the relatively fewer number of variables that are optimized with simple, independent voxel-wise approaches. Besag proposed the iterative conditional modes (ICM) algorithm as an approximation algorithm for discrete MRF optimization (Besag, 1986). That is, the ICM enforces spatial homogeneity by approximating the solution for each voxel independently while fixing the solutions for its neighborhood. Thus, the ICM tends to converge slowly to a sub-optimal solution in the discrete setting (Lempitsky et al., 2010). In the case of a binary field (i.e., the Ising model), graph min-cut techniques are able to pinpoint the globally optimal solution of the energy minimization problem. Further, several combinatorial approximation algorithms were proposed for setting more than two possible labels (i.e., the Potts model). We refer the reader to Szeliski et al. (Szeliski et al., 2008) for a review and comparison of different combinatorial algorithms for the multiple labels case. For inference in continuous MRF models in which each node represents a continuous random variable, the Markov Chain Monte Carlo (MCMC) and the continuous version of the ICM algorithm are commonly used.

In the specific context of parametric MRI, Schmid et al. proposed a Gaussian MRF model with MCMC optimization to increase the reliability of parameter estimates in quantitative, dynamic contrast-enhanced MRI (DCE-MRI) (Schmid et al., 2006). More recently, Kelm et al. proposed a similar Gaussian MRF model with ICM-based optimization in both DCE-MRI (Kelm et al., 2009) and in magnetic resonance spectroscopy (MRS) (Kelm et al., 2012).

To solve the challenging problem of inference of the Incoherent Motion model parameters imposed by incorporating additional spatial homogeneity prior to the previously used IVIM model, we also introduce the “fusion bootstrap moves” (FBM) solver, an efficient new iterative combinatorial solver that, when applied to our new IM model, generates precise parameter estimates. Our FBM solver iteratively updates parameter estimates by applying binary graph-cut solver to fuse the current estimate of parameter values with a new proposal of the parameter values into a new estimate of parameter values that better fit the observed DW-MRI data (Lempitsky et al., 2010). The proposals of parameter values are sampled from the independent voxel-wise distributions of the parameter values with a model-based bootstrap resampling of the residuals (Davidson and Flachaire, 2008).

This paper extends work previously presented at the MICCAI 2012 conference (Freiman et al., 2012b) by offering a more detailed description of the method and additional experiments. Following the Introduction, the paper is organized into 6 sections (2–7). In Section 2, we briefly describe the DW-MRI signal decay model employed, and we review the conventional approach to IVIM parameter estimation. In Section 3, we introduce the spatial homogeneity prior followed by a description of the FBM solver. In Section 4, we describe the experimental methodology, the DW-MRI data for our simulation, and in-vivo experiments. In Section 5, we present results for simulated DW-MRI data as well as in-vivo DW-MRI data from normal abdominal organs of 30 subjects and 3 musculoskeletal lesions studies. In Section 6, we discuss study results as well as limitations; and last, we summarize our findings and the impact of our work in Section 7.

## 2. The Intravoxel incoherent motion model

The Intra-Voxel Incoherent Motion (IVIM) model of DW-MRI signal decay assumes a signal decay function of the form (Le Bihan, 2008; Le Bihan et al., 1988):

$$m_{v,i}=s_{0,v}(f_v \exp(-b_i(D_v^*+D_v))+(1-f_v)\exp(-b_i(D_v))) \quad (1)$$

where  $m_{i,v}$  is the expected signal of voxel  $v$  at  $b$ -value= $b_i$ ,  $s_{0,v}$  is the baseline signal at voxel  $v$ ;  $D_v$  is the slow diffusion decay associated with extravascular water molecules’ motion;  $D_v^*$  is the fast diffusion decay associated with the intravascular water molecules’ motion; and  $f_v$  is the fraction between the slow and fast diffusion compartments.

Given the DW-MRI data acquired with multiple  $b$ -values, the observed signal ( $S_v$ ) at each voxel  $v$  is a vector of the observed signal at the different  $b$ -values:  $S_v = \{s_{v,i}\}$ ,  $i = 1 \dots N$ .

We model the IVIM model parameters at each voxel  $v$  as a continuous-valued four-dimensional random variable (i.e.  $\Theta_v = \{s_{0,v}, f_v, D_v^*, D_v\}$ ). Commonly, the IVIM model parameters  $\Theta_v$  are estimated from the DW-MRI signal  $S_v$  using an independent voxel-wise maximum-likelihood estimator:

$$\widehat{\Theta}_v = \arg \max_{\Theta_v} p(S_v | \Theta_v) = \prod_{i=1}^N p(S_{v,i} | \Theta_v) \quad (2)$$

Assuming the non-central  $\chi$ -distribution noise model that is suitable for parallel MRI acquisitions used in DW-MRI (Dietrich et al., 2008; Brion et al., 2011),  $p(s_{v,i}|\Theta_v)$  takes the following form:

$$p(s_{v,i}|\Theta_v) = \frac{s_{v,i}}{\sigma^2} \left( \frac{m_{v,i}}{s_{v,i}} \right)^{k-1} \exp \left( -\frac{s_{v,i}^2 + m_{v,i}^2}{2\sigma^2} \right) I_{k-1} \left( \frac{s_{v,i} m_{v,i}}{\sigma^2} \right) \quad (3)$$

where,  $\sigma$  being the noise standard deviation of the Gaussian noises present on each of the acquisition channels;  $k$  being the number of channels used in the acquisition; and  $I_{k-1}$  being the  $(k-1)$ <sup>th</sup> order, modified, Bessel function of the first kind. Using a Gaussian approximation of the non-central  $\chi$ -distribution, and taking the negative log of the maximum likelihood estimator; the maximum likelihood estimation takes the form of a least-squares minimization problem:

$$\widehat{\Theta}_v = \arg \min_{\Theta_v} \sum_{i=1}^N (m_{v,i} - s_{v,i})^2 \quad (4)$$

The IVIM model parameters  $\Theta_v$  are estimated from the DW-MRI signal  $S_v$  by solving the least-squares minimization problem (Eq. 4) for each voxel independently using the Levenberg-Marquardt algorithm (Lemke et al., 2011; Yamada et al., 1999).

### 3. Spatial homogeneity prior and the Fusion Bootstrap Moves solver

#### 3.1. Spatial homogeneity prior

Taking the Bayesian perspective, our goal is to find the parametric maps  $\Theta$  that maximize the posterior probability associated with the maps given the observed signal  $S$  and the spatial homogeneity prior knowledge:

$$\widehat{\Theta} = \arg \max_{\Theta} p(\Theta|S) \propto p(S|\Theta)p(\Theta) \quad (5)$$

Based on the Hammersley-Clifford theorem (Winkler, 2003), by using a spatial prior in the form of a continuous-valued Markov random field, the posterior probability  $p(S|\Theta)p(\Theta)$  can be decomposed into the product of node and clique potentials:

$$p(S|\Theta)p(\Theta) \propto \prod_v p(S_v|\Theta_v) \prod_{v_p \sim v_q} p(\Theta_{v_p}, \Theta_{v_q}) \quad (6)$$

where  $p(\Theta_v|S_v)$  is the data term representing the probability of voxel  $v$  to have the DW-MRI signal  $S_v$  given the model parameters  $\Theta_v$ ,  $v_p \sim v_q$  is the collection of the neighboring voxels according to the employed neighborhood system, and  $p(\Theta_{v_p}, \Theta_{v_q})$  is the spatial homogeneity prior in the model.

By taking the negative logarithm of the posterior probability (Eq. 6), the maximum a posteriori (MAP) estimate  $\Theta$  is equivalent to the minimization of:

$$E(\Theta) = \sum_v \varphi(S_v; \Theta_v) + \sum_{v_p \sim v_q} \psi(\Theta_{v_p}, \Theta_{v_q}) \quad (7)$$

where  $\varphi(S_v; \Theta_v)$  and  $\psi(\Theta_{v_p}, \Theta_{v_q})$  are the compatibility functions:

$$\varphi(S_v; \Theta_v) = -\log p(S_v | \Theta_v), \quad \psi(\Theta_{v_p}, \Theta_{v_q}) = -\log p(\Theta_{v_p}, \Theta_{v_q}) \quad (8)$$

The data term  $\varphi(S_v; \Theta_v)$  is given by taking the negative logarithm of Eq. 3, and the spatial homogeneity term is defined using the robust L1-norm:

$$\psi(\Theta_{v_p}, \Theta_{v_q}) = \alpha W |\Theta_{v_p} - \Theta_{v_q}| \quad (9)$$

where  $\alpha \geq 0$  weights the amount of spatial homogeneity enforced by the model, and  $W$  is a diagonal weighting matrix that accounts for the different scales of the parameters in  $\Theta_v$ .

### 3.2. The Fusion Bootstrap Moves solver

The very high dimensionality of the parameters' vector  $\Theta$  of the energy function in Eq. 7 (e.g., the number of voxels in the image multiplied by the number of the signal decay model parameters) makes energy optimization very challenging.

To robustly minimize the energy in Eq. 7, we developed a new solver that harnesses the power of the combinatorial binary graph-cut approach (previously used for discrete MRF optimization) to address the persistent challenges associated with continuous MRF optimization. Our “fusion bootstrap moves (FBM)” algorithm, inspired by the fusion-moves algorithm (Lempitsky et al., 2010), iteratively updates parameter estimates by applying a binary graph-cut solver to fuse the current estimate of parameter values with a new proposal of the parameter values into a new estimate of parameter values that better fit the observed DW-MRI data. The proposals of parameter values are sampled from the independent voxel-wise distributions of the parameter values with a model-based bootstrap resampling of the residuals (Davidson and Flachaire, 2008; Freiman et al., 2011).

Since fusion of the two possible proposals at each iteration is optimal, efficient reduction in the overall model energy (Eq. 7) is guaranteed. By applying the proposal drawing and optimal fusion steps iteratively, the algorithm will robustly converge – at least to a local minimum. Next, we describe these steps in detail.

**3.2.1. Proposal Drawing**—We utilize the model-based bootstrap technique (Davidson and Flachaire, 2008) to draw a new proposal from the empirical distribution of the incoherent motion parameter values as follows: For each voxel  $v$ , the raw residuals between the observed signal ( $S_v$ ) at voxel  $v$  and the expected signal ( $M_v = \{m_{v,j}\}, j = 1, \dots, N$ ) at each b-value  $b_j$ , given the current model estimate ( $\Theta_v^0$ ), are defined as:

$$\varepsilon_{v,i} = m_{v,i} - S_{v,i} \quad (10)$$

The model-based bootstrap resampling is defined as:

$$s_{v,i}^*(\Theta_v^0) = m_{v,i} + t_{v,i} \widehat{\varepsilon}_{v,i} \quad (11)$$

where  $s_{v,i}^*(\Theta_v^0)$  is the resampled measures at b-value  $b_i, i = 1 \dots N$ ,  $\widehat{\varepsilon}_{v,i}$  are the rescaled version of  $\varepsilon_{v,i}$  that accounts for heterogeneous errors leverages (Freiman et al., 2011), and  $t_{v,i}$  is a two-point Rademacher distributed random variable with  $p(t_{v,i} = 1) = 0.5$  and  $p(t_{v,i} = -1) = 0.5$  defined for each voxel and b-value independently (Davidson and Flachaire, 2008).

The new proposal of the IVIM model parameters  $\Theta_v^1$  is then estimated for each voxel independently using Eq. 4.

It should be noted that simply drawing samples from a pre-defined artificial distribution of the parameters is not appropriate as the actual distribution of the parameters is spatially variant (Freiman et al., 2011). Therefore, samples drawn from a pre-defined artificial distribution will slow the optimization as they have a greater chance of being rejected by the graph-cut optimization, compared to samples drawn from the spatially-variant distribution with the bootstrap process.

**3.2.2. Proposal fusion**—We use the binary graph-cut technique (Lempitsky et al., 2010) to find the optimal fusion of the current assignment  $\Theta^0$  and the new proposal  $\Theta^1$  for the IVIM model parameters values that form a new estimate of the parameters maps  $\Theta^*$  which have the lowest possible energy among the possible fusions of  $\Theta^0$  and  $\Theta^1$  as follows:

Let  $G = (V, E)$  be an undirected graph where each voxel  $v$  is represented as a graph node; the two proposals  $\Theta^0$  and  $\Theta^1$  are represented by the terminal nodes  $v_s$  and  $v_t$ ; and graph edges consist of three groups:  $E = \{(v_p, v_q), (v_p, v_s), (v_p, v_t)\}$ . Edge weights  $w(v_p, v_s)$  and  $w(v_p, v_t)$  represent the likelihood of the model parameters  $\Theta^0$  and  $\Theta^1$  given the observed signal  $S_{v,p}$ , respectively:

$$w(v_p, v_s) = \varphi(S_{v,p}; \Theta_v^0), w(v_p, v_t) = \varphi(S_{v,p}; \Theta_v^1) \quad (12)$$

Edge weights  $w(v_p, v_q)$  penalize for adjacent voxels that have different model parameters:

$$w(v_p, v_q) = \psi(\Theta_{v,p}, \Theta_{v,q}) \quad (13)$$

The optimal fusion between  $\Theta^0$  and  $\Theta^1$  that forms the new estimate of the parameter maps  $\Theta^*$  is then found by solving the corresponding graph min-cut problem. Finally, the result  $\Theta^*$  is assigned as  $\Theta^0$  for the next iteration.

Figure 2 depicts the graph set-up for the minimization of energy in Eq. 7.

## 4. Experimental methodology

### 4.1. Hyper-parameter optimization

The spatial homogeneity prior model defines three hyper-parameters: 1) the standard deviation of the signal noise; 2) the parameter weighting matrix  $W$ , and; 3) the spatial smoothness prior weight  $\alpha$ . The standard deviation of the signal noise is estimated from a pre-defined background region for each dataset. All other parameters were previously determined and have been used subsequently for all experiments. Following the methodology of Kelm et al. (Kelm et al., 2009), we determined the values of the diagonal of the parameter weighting matrix as follows: We assessed the scale difference in the IVIM parameter mean values of the main abdominal organs reported by Yamada et al. (Yamada et al., 1999). Next, we set the rescaling matrix  $W$  diagonal to  $\{1.0, 0.001, 0.0001, 0.01\}$  to provide equal weight to each one of the incoherent motion model parameters. We assessed the impact of spatial smoothness prior weight  $\alpha$  on the simulated data as well as on preliminary *in-vivo* DW-MRI data of healthy subjects. According to these preliminary experiments, we set the value of  $\alpha$  to 0.01. We used this value in all of the DW-MRI data analyses presented in this manuscript.

## 4.2. Precision and accuracy of the incoherent motion parameter estimates from simulated DW-MRI data

We conducted a Monte-Carlo simulation study to analyze the estimation errors in incoherent motion quantification from DW-MRI using both the original independent voxel-wise IVIM analysis and our spatially-constrained model. To assess the efficacy of our FBM solver, we have also compared the graph min-cut based fusion against two versions of the ICM algorithm (Besag, 1986): 1) A continuous ICM in which energy minimization is performed for each voxel on the continuous domain with the current estimate of the incoherent motion parameters of the neighboring voxels as constraints (IM-ICM<sub>C</sub>) (Kelm et al., 2009) with the BOBYQA derivative-free, non-linear optimization algorithm proposed by Powell (Powell, 2009), and; 2) a discrete version in which the ICM strategy is used to reach an approximate solution for each fusion problem, but otherwise leaving the entire fusion framework unchanged (IM-ICM<sub>D</sub>) (Lempitsky et al., 2010). We initialized all solvers for our spatially-constrained model with the results of the independent voxel-wise IVIM estimation.

We constructed a simulated heterogeneous tumor example (Kelm et al., 2009) as follows: We defined three-dimensional reference parametric maps with  $100 \times 100 \times 5$  voxels with the following parameters: Border:  $\Theta = \{200, 0.35, 0.03, 0.003\}$ , middle part:  $\Theta = \{200, 0.25, 0.02, 0.002\}$ , innermost part:  $\Theta = \{200, 0.15, 0.01, 0.001\}$ . We computed simulated DW-MRI images from the parametric maps using Eq. 1 with 7 b-values in the range  $[0, 800]$  s/mm<sup>2</sup>. We then corrupted the simulated data by non-central  $\chi$ -distributed noise with single coil noise  $\sigma$  values in the range of 2–16 defined on the same scale as the assumed  $s_0$ , which implies an assumed SNR range of 100–12.5. Fig. 3 depicts the model parameter maps and the simulated noisy DW-MRI images with different b-values at SNR of 25.

We estimated the model parameters  $\Theta$  from the noisy DW-MRI data for each voxel using the following four methods: 1) the voxel-independent approach (IVIM) (Le Bihan, 2008; Le Bihan et al., 1988; Koh et al., 2011); 2) our spatial homogeneity prior model with ICM based continuous optimization (IM-ICM<sub>C</sub>) (Kelm et al., 2009); 3) our spatial homogeneity prior model with ICM fusion strategy (IM-ICM<sub>D</sub>) (Lempitsky et al., 2010), and; 4) our spatial homogeneity prior model with graph min-cut fusion strategy (IM-FBM). The noise parameter  $\sigma$  was estimated using a pre-defined background region. Stopping criteria for all methods (IM-ICM<sub>C</sub>, IM-ICM<sub>D</sub>, IM-FBM) was defined as an energy improvement of less than 0.1% from the initial energy or 500 iterations. Following the methodology of Kelm et al. (Kelm et al., 2009), we calculated the estimator bias, the standard deviation and the relative root mean square (RRMS) error between the reference and estimated parameters for each parameter. We also compared the increase in running time (due to the Bayesian model estimation) in both the FBM and the ICM approaches to the running time of the independent voxel-wise IVIM approach.

## 4.3. Precision of the Incoherent Motion parameter estimates from in-vivo DW-MRI data

We obtained DW-MRI images of 30 subjects - 18 males and 12 females with a mean age of 14.7 (range 5–24, std 4.5) that underwent MRI studies due to suspected inflammatory bowel disease between Sept. 2010 and Sept. 2011. Radiological findings of the study subjects' abdominal organs (i.e., liver, kidneys and spleen) were normal.

We carried out MR imaging studies of the abdomen using a 1.5-T unit (Magnetom Avanto, Siemens Medical Solutions, Erlangen, Germany) with a body-matrix coil and a spine array coil for signal reception. Free-breathing single-shot echo-planar imaging was performed using the following parameters: repetition time/echo time (TR/TE) = 6800/59 ms; SPAIR fat suppression; matrix size = 192×156; field of view = 300×260 mm; number of excitations = 1; slice thickness/gap = 5 mm/0.5 mm; 40 axial slices; 8 b-values =

5,50,100,200,270,400,600,800 s/mm<sup>2</sup>. A tetrahedral gradient scheme, first proposed in Conturo et al. (Conturo et al., 1996), was used to acquire 4 successive images at each b-value with an overall scan acquisition time of 4 min. Diffusion trace-weighted images at each b-value were generated using geometric averages of the images acquired in each diffusion sensitization direction (Mulkern et al., 2001).

We estimated the model parameters  $\Theta$  from the *in-vivo* DW-MRI data for each voxel using both the independent voxel-wise approach IVIM and our IM-FBM approach. We calculated the averaged model parameter  $\Theta$  values obtained using the four different methods over three regions of interest (ROI) - each manually annotated in the liver, spleen, and kidney (Fig. 4). Next, we determined whether there is a statistically significant difference among the average model parameter values estimated with the different estimation methods using a two-tailed, paired Student's t-test, ( $p < .05$  indicating a significant difference). We calculated the precision of the parameter estimates by means of the coefficient of variation (CV) of the parameter estimates at each voxel in the respective IVIM and IM-FBM maps of each patient using model-based wild-bootstrap analysis (Davidson and Flachaire, 2008; Freiman et al., 2011). For each patient, we averaged the CV values over the same three ROIs mentioned above. We examined the statistical significance of the difference in the precision of the parameter estimates for the IVIM and IM-FBM maps using a two-tailed paired Student's t-test ( $p < .05$  indicating a significant difference). We performed the statistical analyses with standard statistical software (Matlab™ R2010b; The MathWorks, Natick, MA, USA).

#### 4.4. Characterization of heterogeneous lesions

We analyzed the characterization of heterogeneous musculoskeletal lesions characterization with our IM-FBM method compared to the IVIM method by means of the contrast-to-noise ratio (CNR) among components of the lesions. Specifically, we examined DW-MRI data of 3 patients with musculoskeletal lesions (2 diagnosed with left femoral osteosarcoma (OS1, OS2), and 1 diagnosed with popliteal cyst (PC) with internal debris in the posterior right calf).

The MRI data was acquired using a 3-T unit (Skyra, Siemens Medical Solutions, Erlangen, Germany). The DW-MRI protocol was as follows: Free-breathing single-shot echo-planar imaging of the lower extremities was performed using the following parameters: repetition time/echo time (TR/TE) = 10425/70 ms; SPAIR fat suppression; matrix size = 128 × 108; field of view = 207×173 mm; number of excitations=5; slice thickness/gap = 4 mm/0.0 mm; 40 axial slices; 5 b-values = 0,50,100,500,800 s/mm<sup>2</sup>. In addition, post contrast T1-weighted MRI images were acquired.

For all cases, an experienced radiologist (K.E.) identified the peripheral rim component and the central part component on the post-contrast, T1-weighted images based on their respective enhancement patterns. Fig. 5 depicts the left femoral osteosarcoma components on the post-contrast, T1-weighted image; on the T2-weighted image; and on the diffusion-weighted image.

We calculated the incoherent motion parametric maps using the IVIM approach and our IM-FBM approach. The internal components were annotated manually on the  $f$  map computed with our IM-FBM approach. We evaluated the improvement in the contrast-to-noise ratio (CNR) by means of Hedges' g effect-size (Hedges, 1981). Specifically, we looked at the differences in  $f$  values among the internal components that resulted from the IVIM and IM-FBM approaches, respectively.

## 5. Experimental results

### 5.1. Precision and accuracy of the incoherent motion parameter estimates from simulated DW-MRI data

Fig. 6 depicts the parametric maps estimated from the simulated DW-MRI data using the IVIM approach as well as our Bayesian approach with spatial homogeneity prior optimized using 1) the continuous ICM method (IM-ICM<sub>C</sub>); 2) the discrete ICM method (IM-ICM<sub>D</sub>) and; 3) the FBM method (IM-FBM).

Fig. 7 presents the relative bias; the relative standard deviation of the estimates error; and the relative root mean square error (RRMS) plots of the incoherent motion parameter estimators as a function of the SNR using the IVIM approach as well as our Bayesian approach with spatial homogeneity prior that were then optimized using the ICM<sub>C</sub>, the ICM<sub>D</sub>, and the proposed FBM methods. The introduction of the spatial homogeneity prior reduced the relative bias, the relative STD and the relative RRMS of the parameter estimates, with the exception of the relative bias in  $f$  estimates using our IM-FBM approach. We observed the greatest improvement in the bias of the estimates in the  $D^*$  parameter where the bias was reduced from ~40% with the IVIM method to 10% using the IM-FBM method, and to ~5% using the IM-ICM<sub>C</sub> and IM-ICM<sub>D</sub> methods in realistic SNR<sub>B0</sub> of 20. With our IM-FBM approach, the relative standard deviation of the estimates error and overall RRMS were reduced by 80% for the  $D^*$  parameter, and by 50% for the  $D$  and  $f$  parameters compared to the IVIM approach in a realistic SNR<sub>B0</sub> scenario of 20.

The running time required to reconstruct the parametric maps of one slice of  $100 \times 100$  voxels on a single processor machine Intel® Xeon® at 2.40GHz with cache size of 12MB were as follows: 1.372 sec for the entire slice (0.137 ms per voxel) using the IVIM approach; 52.9 sec for the entire slice (5.29 ms per voxel) using the IM-ICM<sub>C</sub> approach; 112.8 sec for the entire slice (11.28 ms per voxel) using the IM-ICM<sub>D</sub> approach; and 142.12 sec for the entire slice (14.21 ms per voxel) using the IM-FBM approach.

### 5.2. Precision of the Incoherent Motion parameter estimates from in-vivo DW-MRI data

Fig. 8 depicts a representative example of the incoherent motion parametric maps of the upper abdomen calculated using the two methods (i.e., IVIM and the proposed IM-FBM). By incorporating the spatial homogeneity prior, the quality of the images improved (3<sup>rd</sup> row) compared to the voxel-wise, independent approach (2<sup>nd</sup> row) that resulted in more detailed maps. We also analyzed the signal decay in a noisy point inside the liver vasculature, which is expected to have a significant percentage of the fast-diffusion component (green point in Fig. 8a). While the IVIM model failed to depict the fast-diffusion component in the signal decay, our IM-FBM model successfully captured the fast-diffusion component (Fig. 8c).

Table 1 summarizes the average values of the incoherent motion parameters for each organ's ROI, as estimated by the two methods along with the level of significance of the difference (two-tailed paired Student's t-test, N=30, p<0.05).

Fig. 9 depicts the bar plots of the CV over the 30 subjects for the incoherent motion parameters. Our IM-FBM approach reduced the CV of the  $D^*$  parameter estimates by 43%; the CV of the  $f$  parameter estimates by 37%; and the CV of the  $D$  parameter by 17%. The improvement in CV was significant for all parameters (p<0.0001).

### 5.3. Characterization of heterogeneous lesions

Fig. 10 depicts the incoherent motion parametric maps calculated using the IVIM and our IM-FBM approach. Similar to the results of the simulation and in-vivo experiments, the IM-

FBM approach produced smoother, more realistic parametric maps with improved sensitivity to details seen especially in the  $f$ , and  $D^*$  maps.

Fig 11 compares the results of the IVIM and IM-FBM approaches with bar plots that show the CNR between the lesion's internal components on the  $f$  maps. By using our IM-FBM approach, we achieved an average improvement in the CNR between the two internal components of 19.3% over the IVIM approach.

## 6. Discussion

Incoherent motion quantification from DW-MRI has a promising role as a quantitative non-invasive imaging biomarker for various clinical applications. However, the commonly used independent, voxel-wise fitting of the IVIM model does not account for inter-voxel interactions. Moreover, the low-quality of the incoherent motion parameter estimates using the IVIM model has hampered its utilization in clinical studies and in patient management (Koh et al., 2011).

In this work, we introduced a new model of DW-MRI signal decay that accounts for both inter- and intra-voxel incoherent motion by formulating a Bayesian incoherent motion model with spatial homogeneity prior. As a result, our model significantly improved both the visual quality and the precision of incoherent motion parameter estimates without increasing overall scanning times.

Inferring model parameters with a spatial prior is a challenging task, however. Previously, Schmid et al. used MCMC optimization to reliably infer kinetic model parameters from DCE-MRI (Schmid et al., 2006), and Kelm et al. used ICM-based optimization to infer model parameters in both DCE-MRI (Kelm et al., 2009) and MRS (Kelm et al., 2012).

The MCMC approach relies on Markov Chain Monte-Carlo simulation to estimate the prior distributions for all unknown parameters simultaneously, which is very time-consuming. In contrast, the ICM approach only *approximates* the fully Bayesian assumption by estimating the model parameters at each voxel with the current values of the local neighborhood as constraints. Similar to the ICM approach, our FBM solver does not require prior specification of the prior distribution of the entire set of parameters. However, it does apply the fully Bayesian assumption by utilizing global optimization steps with the binary graph-cut approach.

As the simulation experiments demonstrated, our FBM approach provides superior estimates of the incoherent motion model parameters (i.e., a lower standard deviation of errors and overall RRMS) than does the ICM approach in both its continuous and discrete versions. The estimated distribution of residuals using FBM is, moreover, reliable in the presence of realistic levels of noise (SNR = 20) for all parameter values, as it provides globally optimal parameter updates; whereas, ICM provides only locally optimal parameter updates. The local estimates of ICM were inferior in all cases except for estimates of the  $f$  parameter at very high noise levels, where the local nature of the updates may provide some insensitivity to noise.

Compared to the ICM approach, our method was subject to greater bias in estimating parameters owing to a bias in the wild-bootstrap process used to draw samples from the distribution of parameters. In practice, however, the ability to reach precise estimates is more critical to generating detailed maps and thus, to assessing differences among patient groups.

We showed improved quality of the incoherent motion parametric maps on in-vivo DW-MRI data of 30 patients using the CV as the quantitative precision measure. We also demonstrated improved characterization of heterogeneous lesions by means of CNR on DW-MRI data of 3 patients with musculoskeletal lesions. Our method achieved an average improvement of 19.3% in the CNR compared to the IVIM approach, which suggests the improved capability of the  $f$  parameter to distinguish among lesion components.

Our FBM approach has two major advantages: First, it does not assume any specific noise model in estimating the distribution of residuals, and thus can accommodate both acquisition noise and motion-related artifacts. Second, our method does not involve the calculation of derivatives, and thus can be coupled directly with robust spatial priors including the L1 norm employed in this study. The Bayesian estimation that is used in both our FBM and  $ICM_D$  approaches requires  $\sim 100$  fold increase in running time on a single processor compared to the IVIM approach. The  $ICM_C$  approach provided much faster running time, but at the cost of reduced precision. Fortunately, the computation can be performed offline and accelerated using the multi-core machines to which we have access. The radiologist can also limit map calculations to relatively small regions of interest to keep the overall computation time as small as possible.

While we used the FBM method to optimize a Bayesian model of incoherent motion from DW-MRI data; it can be applied to other parametric MRI reconstruction problems as well, including the estimation of kinetic parameters from DCE-MRI and quantitative T1 from T1-weighted MRI.

Our study had several limitations. First, since this manuscript focuses on the technical aspects of reliable estimation of incoherent motion maps, we showed improvements in parametric map quality in both simulated experiments and in the in-vivo data of 30 study subjects. In addition, we demonstrated improvements in the characterization of heterogeneous musculoskeletal lesions on the  $f$  maps of 3 patients. Although our ability to estimate incoherent motion parameters with greater precision and to better characterize heterogeneous lesions has been established in this study, the actual clinical impact has yet to be determined. This requires a large clinical study that utilizes a head-to-head comparison of the decisions reached with IVIM and IM-FBM parametric maps, respectively, in defined patient populations.

Second, this study population was limited by the number of patients and by their age range. As a result, our assessment of DW-MRI data was restricted to the abdominal organs in 30 pediatric patients and to musculoskeletal lesions in 3 pediatric patients.

Third, the DW-MRI acquisition protocols for the study data were limited to those protocols routinely used by our institution. As a result, we employed a fixed set of b-values for the 30 patients who underwent abdominal scan, and a different set with a reduced number of b-values for the musculoskeletal lesions data. An additional study should evaluate the impact of the b-values selected (i.e., by means of values and number of b-values) on the estimated parameters as demonstrated by Lemke et al (Lemke et al., 2011) and Zhang et al. (Zhang et al., 2012).

Fourth, while our experiments show that the maps produced with our method are not “over-smoothed”, the actual amount of qualitative and quantitative smoothing (i.e., the value of the hyper-parameter  $\alpha$ ) should be determined in the setting of a new clinical study aimed at exploring the utility of IM-FBM maps in specific clinical applications.

## 7. Conclusion

The role of incoherent motion parameters as quantitative imaging biomarkers for various clinical applications is becoming increasingly important. However, current techniques for estimating the incoherent motion parameters from DW-MRI data do not provide reliable or specific enough parameter estimates.

In this work, we improved the reliability of incoherent motion measurements from DW-MRI data significantly by introducing a model of DW-MRI signal decay that accounts for both inter- and intra-voxel incoherent motion by incorporating a spatial homogeneity prior.

In addition, we developed a novel method to infer the parameters in the new model by updating parameter estimates iteratively with a binary graph-cut solver that fuses the current estimate of parameter values with a new proposal of the parameter values. This is drawn using model-based residual bootstrap resampling into a new estimate of parameter values that better fit the observed DW-MRI data.

Using our IM model and FBM solver with simulated data, we were able to show improvements in the *in-vivo* abdominal DW-MRI data of 30 patients as well as the *in-vivo* DW-MRI data of 3 patients with musculoskeletal lesions. The IM model, combined with the FBM solver, provides a more precise estimate of the physiological model parameter values that describe the DW-MRI signal decay and a better mechanism for characterizing heterogeneous lesions than does the independent, voxel-wise IVIM model.

## Acknowledgments

This investigation was supported in part by NIH grants R01 EB008015, R01 LM010033, R01 EB013248, and P30 HD018655 and by a research grant from the Boston Children's Hospital Translational Research Program. The authors thank Nancy Drinan for her support in editing this manuscript, and the anonymous reviewers for their insightful comments that helped improve this paper.

## References

- Behrens TE, Woolrich MW, Jenkinson M, Johansen-Berg H, Nunes RG, Clare S, Matthews PM, Brady JM, Smith SM. Characterization and propagation of uncertainty in diffusion-weighted MR imaging. *Magn Reson Med*. 2003; 50 (5):1077–88. [PubMed: 14587019]
- Besag J. On the statistical analysis of dirty pictures. *Journal of the Royal Statistical Society*. 1986; B-48:259–302.
- Brion V, Poupon C, Riff O, Aja-Fernandez S, Tristan-Vega A, Mangin JF, Le Bihan D, Poupon F. Parallel MRI noise correction: an extension of the LMMSE to non central chi distributions. *Med Image Comput Comput Assist Interv*. 2011; 14(Pt 2):226–33. [PubMed: 21995033]
- Chandarana H, Lee VS, Hecht E, Taouli B, Sigmund EE. Comparison of biexponential and monoexponential model of diffusion weighted imaging in evaluation of renal lesions: preliminary experience. *Invest Radiol*. 2011; 46 (5):285–91. [PubMed: 21102345]
- Conturo TE, McKinsty RC, Akbudak E, Robinson BH. Encoding of anisotropic diffusion with tetrahedral gradients: a general mathematical diffusion formalism and experimental results. *Magn Reson Med*. 1996; 35 (3):399–412. [PubMed: 8699953]
- Davidson R, Flachaire E. The wild bootstrap, tamed at last. *Journal of Econometrics*. 2008; 146 (1): 162–169.
- Dietrich O, Raya JG, Reeder SB, Ingrisch M, Reiser MF, Schoenberg SO. Influence of multichannel combination, parallel imaging and other reconstruction techniques on MRI noise characteristics. *Magn Reson Imaging*. 2008; 26 (6):754–62. [PubMed: 18440746]
- Freiman M, Perez-Rossello JM, Callahan MJ, Bittman M, Mulkern RV, Bousvaros A, Warfield SK. Characterization of fast and slow diffusion from diffusion-weighted MRI of pediatric Crohn's

disease. *J Magn Reson Imaging*. 2013 Jan; 37(1):156–63. doi: 10.1002/jmri.23781. [PubMed: 22927342]

- Freiman M, Voss SD, Mulkern RV, Perez-Rossello JM, Warfield SK. Quantitative body DW-MRI biomarkers uncertainty estimation using unscented wild-bootstrap. *Med Image Comput Comput Assist Interv*. 2011; 14(Pt 2):74–81. [PubMed: 21995015]
- Freiman M, Voss SD, Mulkern RV, Perez-Rossello JM, Callahan MJ, Warfield SK. Reliable assessment of perfusivity and diffusivity from diffusion imaging of the body. *Med Image Comput Comput Assist Interv*. 2012; 15(Pt 1):1–9. [PubMed: 23285528]
- Geman S, Geman D. Stochastic relaxation, gibbs distributions, and the bayesian restoration of images. *IEEE Trans Pattern Anal Mach Intell*. 1984; 6 (6):721–41. [PubMed: 22499653]
- Gloria C, Li Q, Xu L, Zhang W. Differentiation of diffusion coefficients to distinguish malignant and benign tumor. *J Xray Sci Technol*. 2010; 18 (3):235–49. [PubMed: 20714083]
- Hedges L. Distribution Theory for Glass's Estimator of Effect Size and Related Estimators. *Journal of Educational Statistics*. 1981; 6 (2):107–128.
- Kelm BM, Kaster FO, Henning A, Weber MA, Bachert P, Boesiger P, Hamprecht FA, Menze BH. Using spatial prior knowledge in the spectral fitting of MRS images. *NMR Biomed*. 2012; 25 (1): 1–13. [PubMed: 21538636]
- Kelm BM, Menze BH, Nix O, Zechmann CM, Hamprecht FA. Estimating kinetic parameter maps from dynamic contrast-enhanced MRI using spatial prior knowledge. *IEEE Trans Med Imaging*. 2009; 28 (10):1534–47. [PubMed: 19369150]
- Klauss M, Lemke A, Grunberg K, Simon D, Re TJ, Wente MN, Laun FB, Kauczor HU, Delorme S, Grenacher L, Stieltjes B. Intravoxel incoherent motion MRI for the differentiation between mass forming chronic pancreatitis and pancreatic carcinoma. *Invest Radiol*. 2011; 46 (1):57–63. [PubMed: 21139505]
- Koh DM, Collins DJ, Orton MR. Intravoxel incoherent motion in body diffusion-weighted MRI: reality and challenges. *AJR Am J Roentgenol*. 2011; 196 (6):1351–61. [PubMed: 21606299]
- Le Bihan D. Intravoxel incoherent motion perfusion MR imaging: a wake-up call. *Radiology*. 2008; 249 (3):748–52. [PubMed: 19011179]
- Le Bihan D, Breton E, Lallemand D, Aubin ML, Vignaud J, Laval-Jeantet M. Separation of diffusion and perfusion in intravoxel incoherent motion MR imaging. *Radiology*. 1988; 168 (2):497–505. [PubMed: 3393671]
- Lemke A, Laun FB, Klauss M, Re TJ, Simon D, Delorme S, Schad LR, Stieltjes B. Differentiation of pancreas carcinoma from healthy pancreatic tissue using multiple b-values: comparison of apparent diffusion coefficient and intravoxel incoherent motion derived parameters. *Invest Radiol*. 2009; 44 (12):769–75. [PubMed: 19838121]
- Lemke A, Stieltjes B, Schad LR, Laun FB. Toward an optimal distribution of b values for intravoxel incoherent motion imaging. *Magn Reson Imaging*. 2011; 29 (6):766–76. [PubMed: 21549538]
- Lempitsky V, Rother C, Roth S, Blake A. Fusion moves for Markov random field optimization. *IEEE Trans Pattern Anal Mach Intell*. 2010; 32 (8):1392–405. [PubMed: 20558873]
- Luciani A, Vignaud A, Cavet M, Nhieu JT, Mallat A, Ruel L, Laurent A, Deux JF, Brugieres P, Rahmouni A. Liver cirrhosis: intravoxel incoherent motion MR imaging—pilot study. *Radiology*. 2008; 249 (3):891–9. [PubMed: 19011186]
- Mulkern RV, Vajapeyam S, Robertson RL, Caruso PA, Rivkin MJ, Maier SE. Biexponential apparent diffusion coefficient parametrization in adult vs newborn brain. *Magn Reson Imaging*. 2001; 19 (5):659–68. [PubMed: 11672624]
- Neil JJ, Bretthorst GL. On the use of Bayesian probability theory for analysis of exponential decay data: an example taken from intravoxel incoherent motion experiments. *Magn Reson Med*. 1993; 29 (5):642–7. [PubMed: 8505900]
- Patel J, Sigmund EE, Rusinek H, Oei M, Babb JS, Taouli B. Diagnosis of cirrhosis with intravoxel incoherent motion diffusion MRI and dynamic contrast-enhanced MRI alone and in combination: preliminary experience. *J Magn Reson Imaging*. 2010; 31 (3):589–600. [PubMed: 20187201]
- Powell, M. Tech rep, technical report NA2009/06, Dep App Math and Th Physics. Cambridge, England: 2009. The BOBYQA algorithm for bound constrained optimization without derivatives.

- Re TJ, Lemke A, Klauss M, Laun FB, Simon D, Grunberg K, Delorme S, Grenacher L, Manfredi R, Mucelli RP, Stieltjes B. Enhancing pancreatic adenocarcinoma delineation in diffusion derived intravoxel incoherent motion f-maps through automatic vessel and duct segmentation. *Magn Reson Med*. 2011; 66 (5):1327–32. [PubMed: 21437979]
- Schmid VJ, Whitcher B, Padhani AR, Taylor NJ, Yang GZ. Bayesian methods for pharmacokinetic models in dynamic contrast-enhanced magnetic resonance imaging. *IEEE Trans Med Imaging*. 2006; 25 (12):1627–36. [PubMed: 17167997]
- Sigmund EE, Cho GY, Kim S, Finn M, Moccaldi M, Jensen JH, Sodickson DK, Goldberg JD, Formenti S, Moy L. Intravoxel incoherent motion imaging of tumor microenvironment in locally advanced breast cancer. *Magn Reson Med*. 2011; 65 (5):1437–47. [PubMed: 21287591]
- Stejskal E, Tanner J. Spin diffusion measurements: spin-echo in the presence of a time dependent field gradient. *J Chem Phys*. 1965; 42:288292.
- Szeliski R, Zabih R, Scharstein D, Veksler O, Kolmogorov V, Agarwala A, Tappen M, Rother C. A comparative study of energy minimization methods for Markov random fields with smoothness-based priors. *IEEE Trans Pattern Anal Mach Intell*. 2008; 30 (6):1068–80. [PubMed: 18421111]
- Winkler, G. *Image Analysis, Random Fields and Dynamic Monte Carlo Methods*. 2. Springer; New York: 2003.
- Yamada I, Aung W, Himeno Y, Nakagawa T, Shibuya H. Diffusion coefficients in abdominal organs and hepatic lesions: evaluation with intravoxel incoherent motion echo-planar MR imaging. *Radiology*. 1999; 210 (3):617–23. [PubMed: 10207458]
- Zhang JL, Sigmund EE, Rusinek H, Chandarana H, Storey P, Chen Q, Lee VS. Optimization of b-value sampling for diffusion-weighted imaging of the kidney. *Magn Reson Med*. 2012; 67 (1):89–97. [PubMed: 21702062]

1. DW-MRI signal decay model that accounts for both inter- and intra-voxel incoherent motion of water molecules by introducing a model of spatial homogeneity
2. Fusion bootstrap moves solver to reliably infer the incoherent motion model parameters
3. Increased precision of Incoherent Motion parameter estimates from in-vivo DW-MRI
4. Improved characterization of heterogeneous tumor environment with Incoherent Motion parametric maps

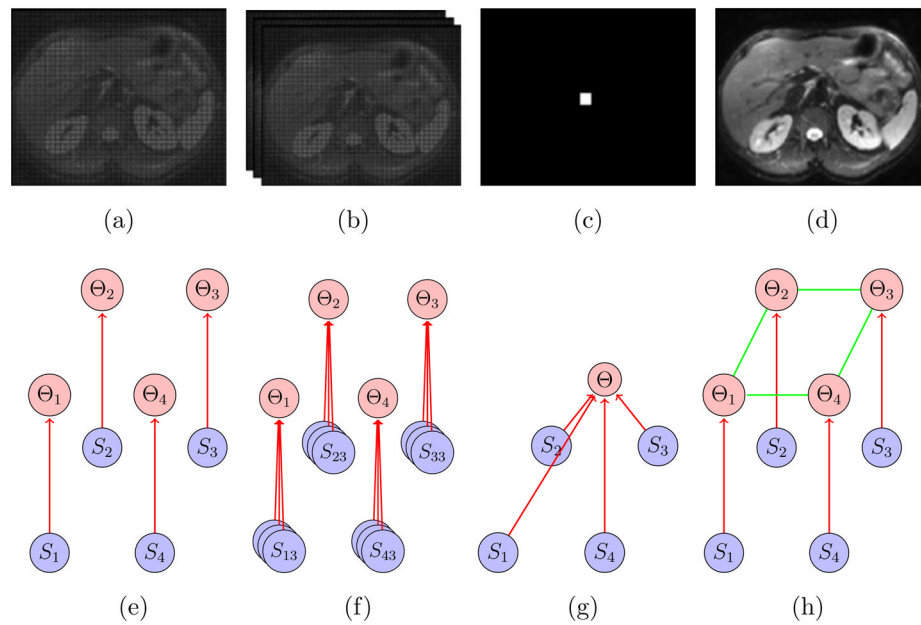
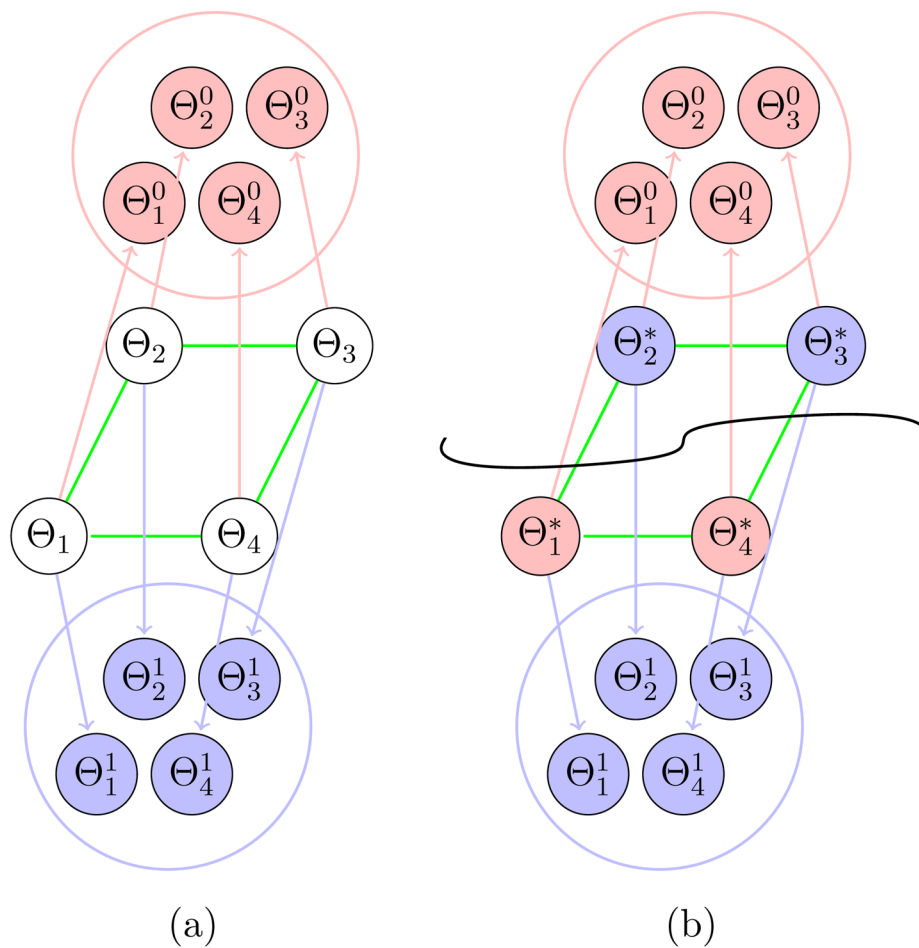
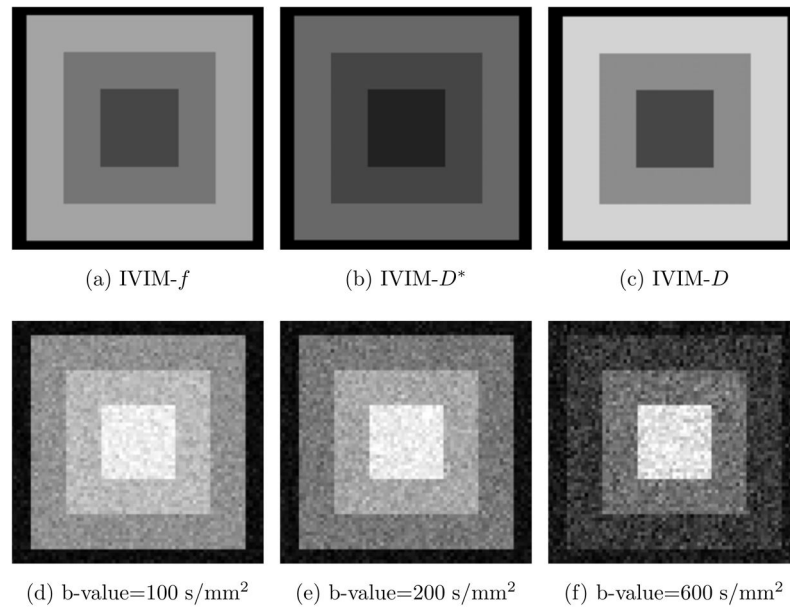
**Figure 1.**

Illustration of the graphical models used to estimate the fast and slow diffusion parameters from DW-MRI data. The first column (a, e) represents independent voxel-wise estimation of intra-voxel incoherent motion; the second column (b, f) represents independent voxel-wise estimation of intra-voxel incoherent motion with multiple DW-MRI images averaged; the third column (c, g) represents estimation of intra-voxel incoherent motion parameters by averaging the DW-MRI signal over a region of interest, and; the fourth column (d, h) represents voxel-wise estimation of the DW-MRI signal decay model parameters that accounts for both inter- and intra-voxel incoherent motion by introducing spatial homogeneity prior.



**Figure 2.** Illustration of the graph configuration used to fuse the proposals of parameter values proposals ( $\Theta^0$ ,  $\Theta^1$ ) into a new estimate of the parameter maps  $\Theta^*$  in an optimal manner with the graph min-cut approach. (a) The graph set-up with unknown parameter estimates  $\Theta$ , and; (b) after the assignment of the new proposals to the variables  $\Theta$  to form the new estimate of the parameter maps  $\Theta^*$ .



**Figure 3.** The heterogeneous tumor example. The first row depicts the reference parametric maps of  $f$ ,  $D^*$ , and  $D$ . The second row depicts representative simulated noisy DW-MRI images generated from the reference parametric maps using Eq. 1.

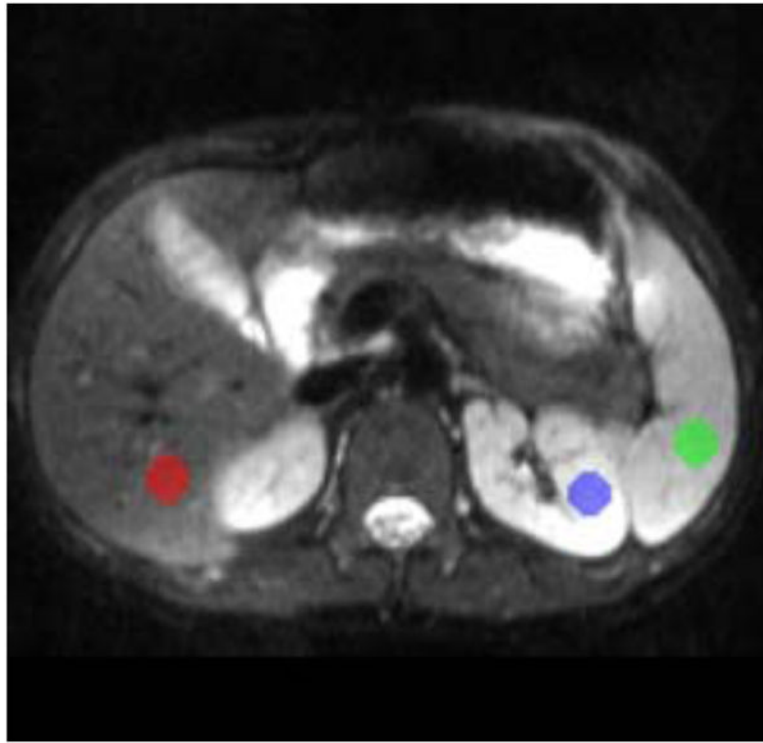


**Figure 4.** Representative example of the regions of interest used to analyze the fit quality overlaid on the DW-MRI image with  $b\text{-value}=5\text{ s/mm}^2$

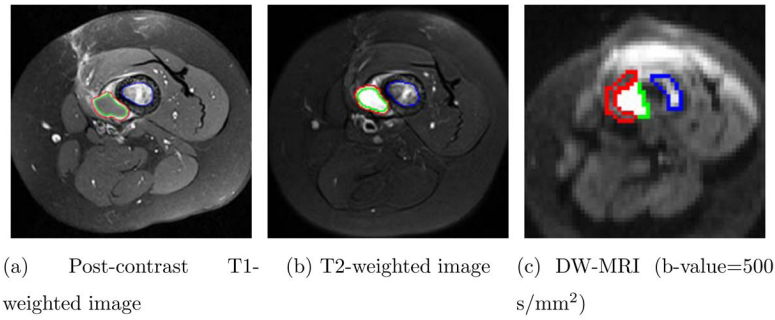


**Figure 5.**

MRI images of heterogeneous femoral diaphyseal osteosarcoma (OS1). There are 3 tumor components: Red - peripheral rim of the soft tissue component (Spr); Green - central part of the soft-tissue component (Sc); and Blue - intramedullary part of the tumor.

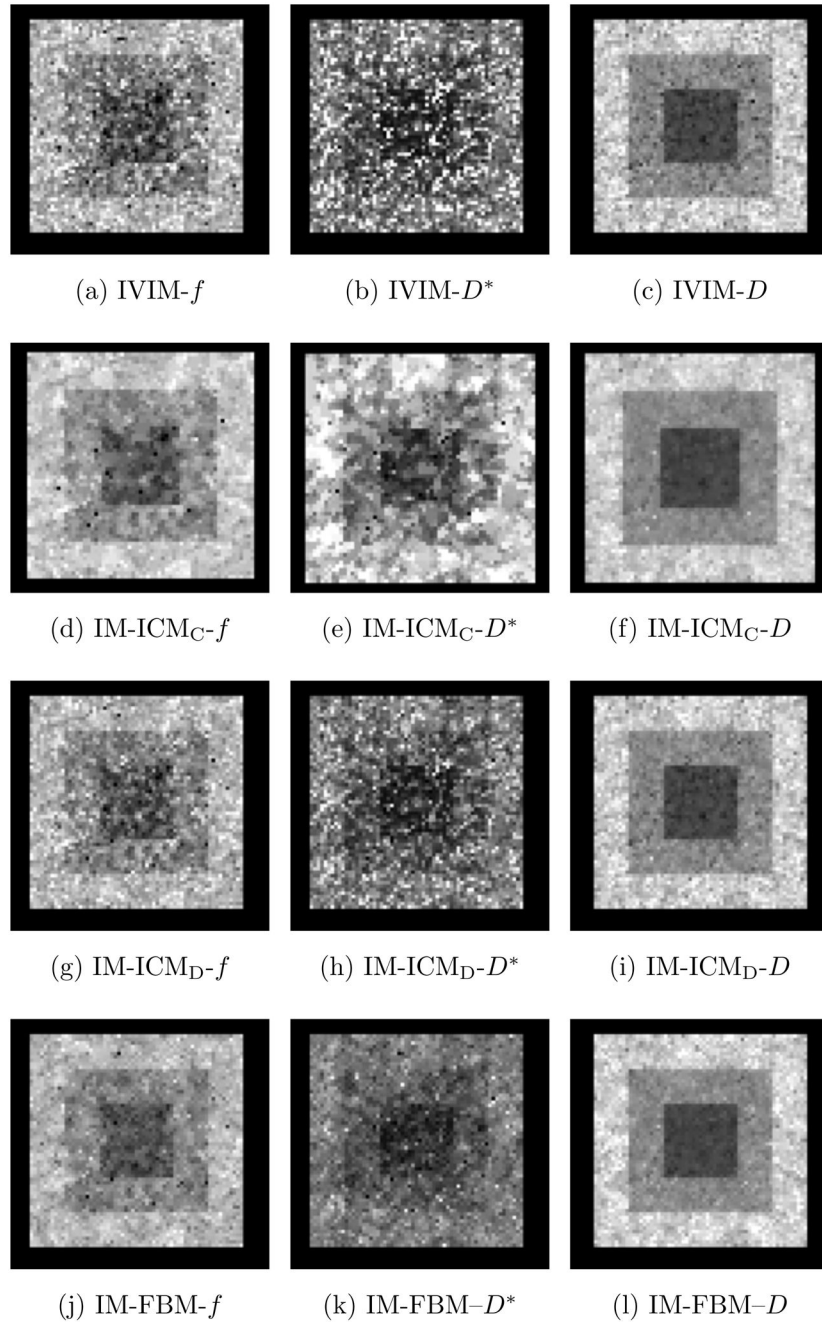


**Figure 6.**

Heterogeneous tumor example results. The first row depicts the incoherent motion parametric maps ( $f$ ,  $D^*$ , and  $D$ ) calculated using the IVIM approach; the second row depicts the maps calculated using the  $ICM_C$  approach; the third row depicts the maps calculated using the  $ICM_D$  approach; and the fourth row depicts the maps calculated using the IM-FBM approach. The Bayesian model (2<sup>nd</sup>-4<sup>th</sup> rows) yields smoother, more realistic maps than does the IVIM approach (1<sup>st</sup> row). Images are presented in the gray-value range as in Fig. 3 for comparison.

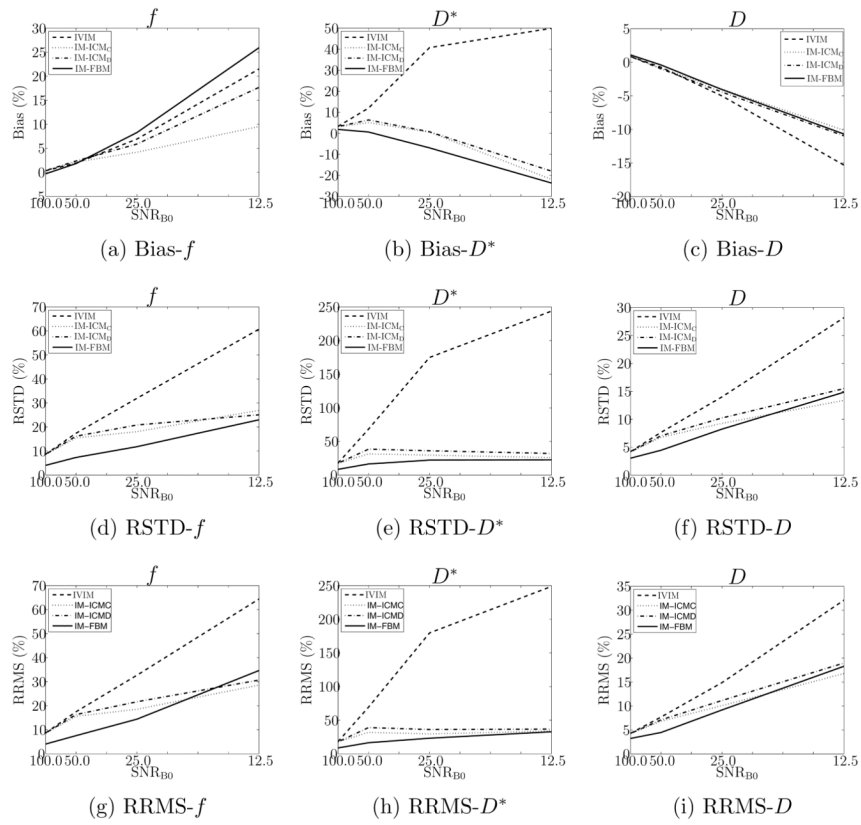


**Figure 7.** Performance of incoherent motion parameter estimators. The first row depicts the bias of each of the estimators used to estimate the incoherent motion model parameters (i.e., IVIM, IM-ICM<sub>C</sub>, IM-ICM<sub>D</sub>, and the proposed IM-FBM). The first row depicts the accuracy of each estimator by means of overall relative bias; the second row depicts the precision of each estimator by means of the relative standard deviation of the estimate errors; and the third row depicts the overall RRMS of each estimator. The introduction of the spatial homogeneity prior improved both the accuracy and precision of the parameter estimates. Under a realistic SNR<sub>B0</sub> scenario of 20, the proposed IM-FBM approach yielded the most precise estimates for all parameters.

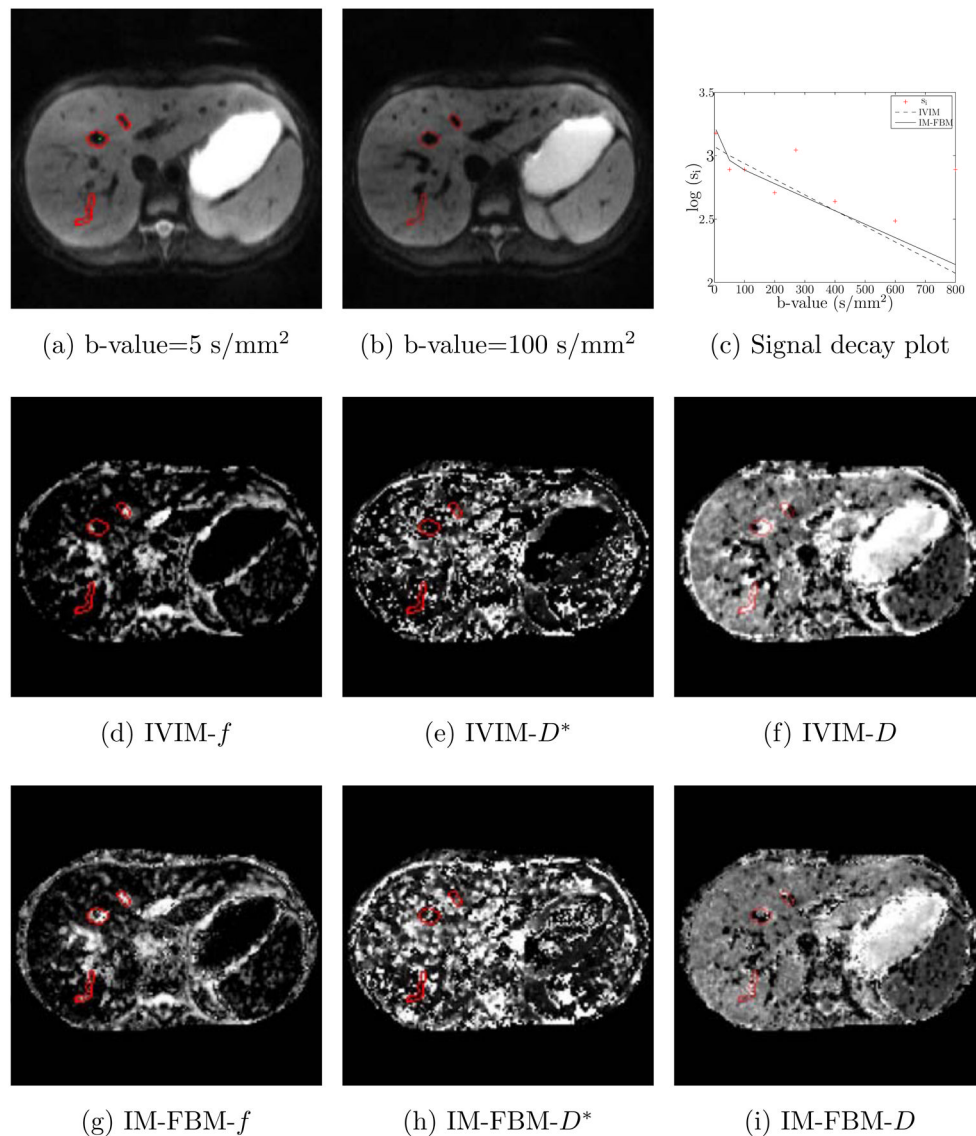


**Figure 8.** Representative DW-MRI and incoherent motion parametric maps of the upper abdomen. (a–b) DW-MRI images, blood vessels inside the liver are encircled in red. (c) DW-MRI signal decay plot of a voxel marked in green in (a). The IVIM model failed to depict the fast-diffusion component in the signal decay due to the noise, while the IM-FBM model successfully captured the fast-diffusion component. (d–f) The incoherent motion parametric maps calculated using the IVIM approach. (g–i) The incoherent motion parametric maps calculated using our IM-FBM approach. Our Bayesian model (3<sup>rd</sup> row) yields parametric maps with more accurate structure compared to the IVIM approach (2<sup>nd</sup> row), especially with respect to the  $f$  parameter. Specifically, the IVIM- $f$  parametric map failed to determine the presence of a fast-diffusion component due to the blood flow, while the IM-FBM approach successfully captured a fast-diffusion component.

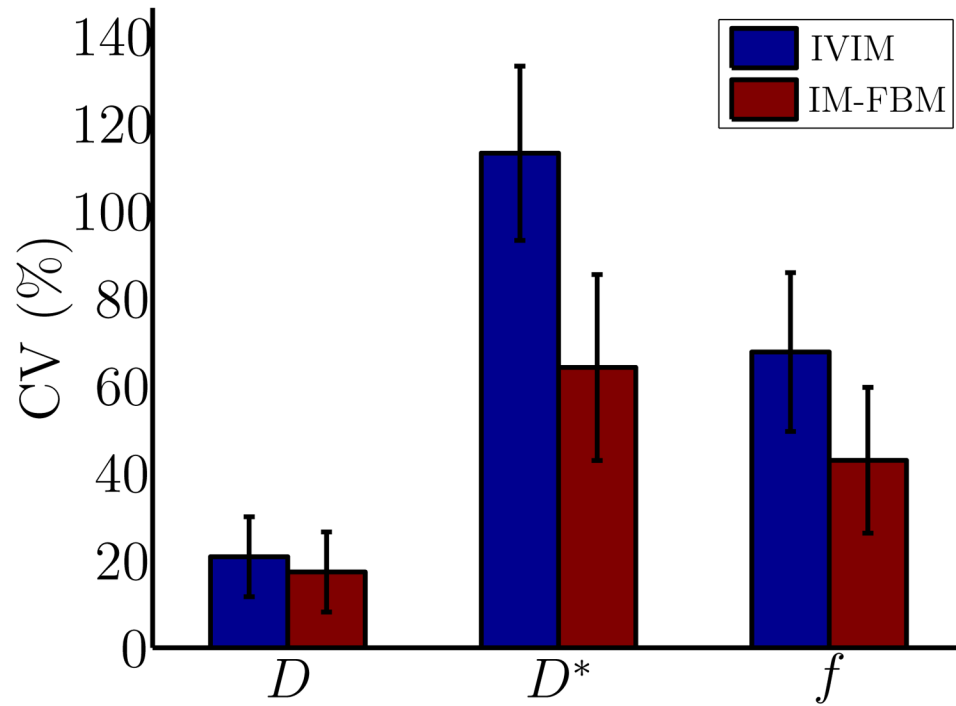


**Figure 9.** Bar plot of the CV of the incoherent motion parameters as estimated from 30 patients. The CV was significantly lower ( $p < 0.0001$ ) when using our IM-FBM approach than when using the IVIM approach for all parameters.

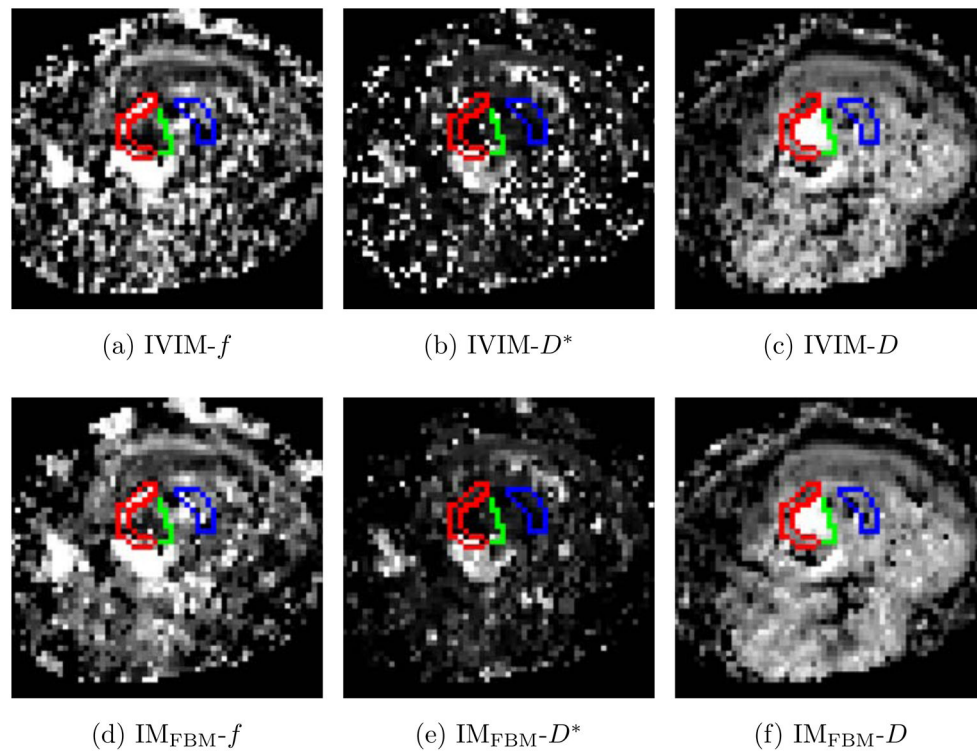


**Figure 10.**

The incoherent motion parametric maps of an osteosarcoma tumor as calculated using the IVIM approach (first row) and our IM-FBM approach (second row) with internal tumor components encircled. The IM-FBM approach produced smoother, more realistic maps than did the IVIM approach.

## Lesions' internal components CNR

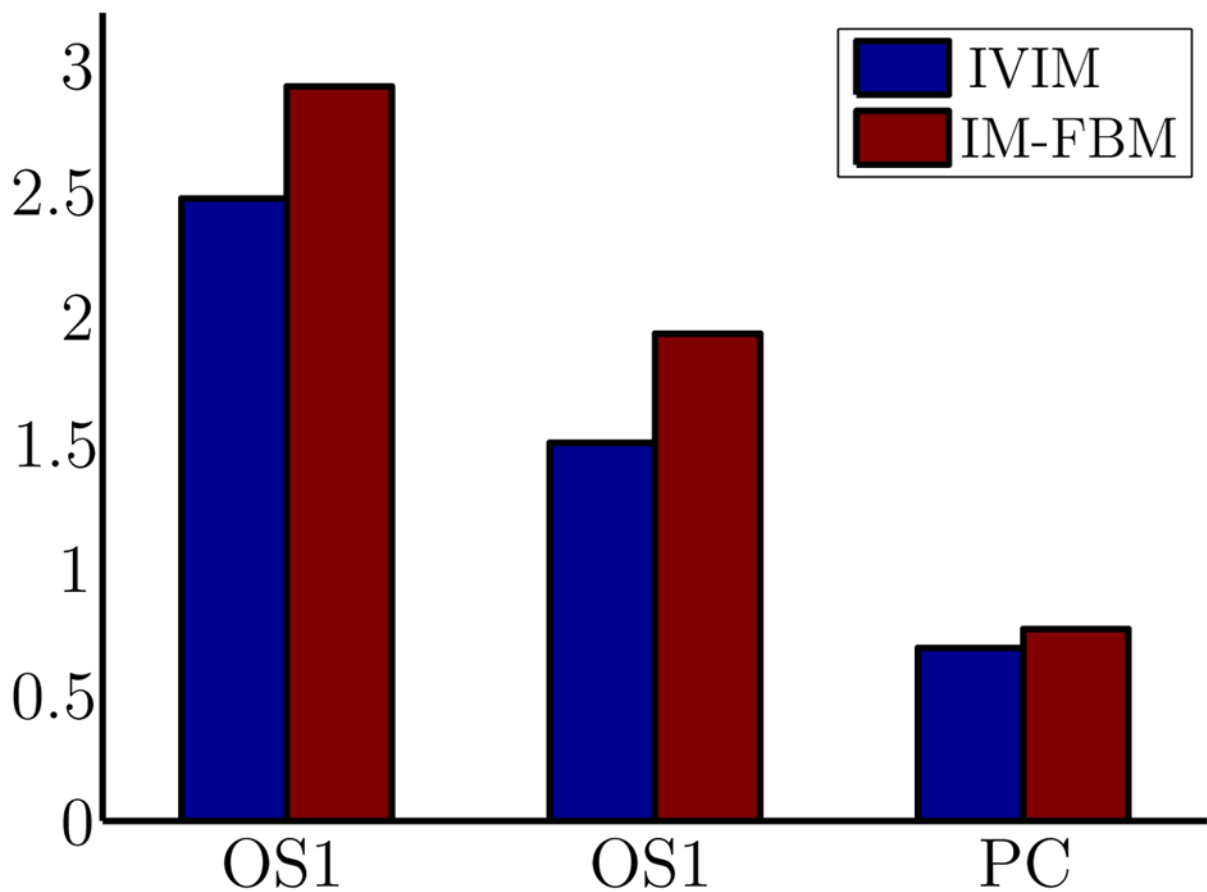


**Figure 11.**

Bar plot of the CNR between the two lesion's internal components on the  $f$  maps as achieved by the IVIM approach (blue) and by our IM-FBM approach (red). With our IM-FBM approach, we achieved an average improvement in the CNR between the two internal components of 19.3% over the IVIM approach.

Table 1

Incoherent motion model parameters values (mean, std) for each organ as calculated using the IVIM and the IM-FBM methods.

	<i>D</i>			<i>D</i> *			<i>f</i>		
	mean	std		mean	std		mean	std	
IVIM	1.02	0.32		41.22	26.58		0.25	0.1	
IM-FBM	0.95	0.26		34.43	36.22		0.28	0.1	
Liver			<b>0.0011</b>			<b>0.0254</b>			<b>&lt;0.001</b>
IVIM	0.91	0.56		20.74	18.25		0.1	0.08	
IM-FBM	0.82	0.37		21.04	31.44		0.13	0.09	
Spleen			<b>0.0297</b>			0.947			<b>0.0045</b>
IVIM	1.76	0.32		23.58	26.72		0.19	0.12	
IM-FBM	1.73	0.3		21.82	30.16		0.21	0.12	
Kidney			<b>0.0152</b>			0.1371			<b>0.0082</b>